Electron Transfer

DOI: 10.1002/anie.201209513

Charge Dynamics in A Donor–Acceptor Covalent Organic Framework with Periodically Ordered Bicontinuous Heterojunctions**

*Shangbin Jin, Xuesong Ding, Xiao Feng, Mustafa Supur, Ko Furukawa, Seiya Takahashi, Matthew Addicoat, Mohamed E. El-Khouly, Toshikazu Nakamura, Stephan Irle, Shunichi Fukuzumi, Atsushi Nagai, and Donglin Jiang**

The donor–acceptor heterojunction is a key structure in current technologies, including transistors, light-emitting diodes, and photovoltaics, because it controls the charge dynamics in the devices.[1–3] Covalent organic frameworks (COFs) are crystalline molecular skeletons that allow atomically precise integration of building blocks into periodic array structures.[4–12] In this regard, we have demonstrated arene, porphyrin, and phthalocyanine COFs that provide periodically ordered columnar arrays of π-components and show outstanding semiconducting and photoconductive properties.[6] We recently synthesized a donor–acceptor COF[6i] that gives rise to a periodically ordered bicontinuous heterojunction structure and self-sorted donor and acceptor columnar arrays separated at nanometer-scale intervals. This nanoscopic segregation morphology forms a broad interface for charge separation, provides ambipolar pathways for charge collection, and would be ideal for the current semiconducting devices that involve photoenergy transformations; however, the charge dynamics, which is a key mechanism that controls the energy transformation, remains unclear.

Here, we report the charge dynamics of a donor–acceptor COF, which were determined using time-resolved spectroscopy to elucidate the photochemical processes of the free charges from their generation to delocalization and retention. In the COF, the heterojunctions allow an ultrafast electron transfer from the donor to the acceptor columns. Consequently, the light absorption is directly coupled with charge dissociation to generate free charges in the donor and acceptor π-columns within 2 ps. On the other hand, the stacked π-columns delocalize the charges, suppress charge recombination, and retain the charges for a prolonged period of time. We show that both solvated and solid-state COFs enable rapid charge separation and exceptional long-term charge retention, thereby providing a key mechanistic basis to envisage the high potential of donor–acceptor COFs for photoelectric applications.

The donor–acceptor COF (Scheme 1a, D_{ZnPc}-A_{NDI}-COF) is a tetragonal, mesoporous 2D framework that is composed of zinc phthalocyanine as an electron donor and naphthalene diimide as an acceptor. In the COF, the two π-units are alternately linked within an electron-transfer distance and at a dihedral angle of approximately 42°. The COF provides self-sorted, bicontinuous columnar arrays and constitutes periodically structured heterojunctions in which each donor column is interfaced with four acceptor columns that are equally active in capturing photo-generated electrons (Scheme 1b). The D_{ZnPc}-A_{NDI}-COF absorbs light over a broad visible and near-infrared region up to 1100 nm (Figure S1 in the Supporting Information). Elemental analysis, infrared spectroscopy, nuclear magnetic resonance spectroscopy, and electron microscopy confirmed the formation of the COF (Figure S2–S4 and Table S1). The same COF has been reported as a thin film.[8c]

The D_{ZnPc}-A_{NDI}-COF exhibited a type IV nitrogen sorption curve that is characteristic of mesoporous frameworks (Figure 1a). The Brunauer–Emmett–Teller surface area and pore volume were calculated as 1410 $m^2 g^{-1}$ and 1.25 $cm^3 g^{-1}$, respectively. The pore-size distribution profile with a range up

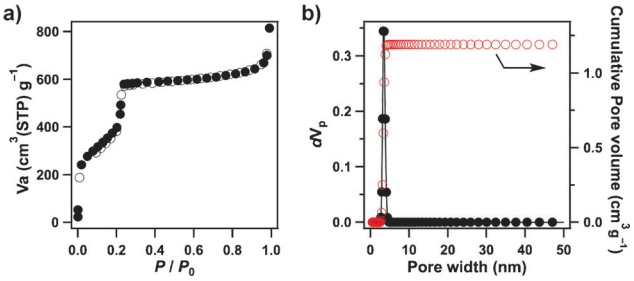

Figure 1. a) Nitrogen sorption isotherm curves measured at 77 K. Filled black circles represent adsorption and the open circles represent desorption. b) Pore-size (black) and pore-size distribution profiles (red).

[*] S. Jin, X. Ding, X. Feng, Dr. K. Furukawa, S. Takahashi, Prof. Dr. T. Nakamura, Dr. A. Nagai, Prof. Dr. D. Jiang
Department of Materials Molecular Science
Institute for Molecular Science
National Institutes of Natural Sciences
5-1 Higashiyama, Myodaiji, Okazaki 444-8787 (Japan)
E-mail: jiang@ims.ac.jp

M. Supur, Prof. Dr. M. E. El-Khouly,[+] Prof. Dr. S. Fukuzumi
Department of Applied Chemistry
Graduate School of Engineering, Osaka University
2-1 Yamadaoka, Suita, Osaka 565-0871 (Japan)

Dr. M. Addicoat, Prof. Dr. S. Irle
Department of Chemistry, Graduate School of Science, Nagoya University
Furo-cho, Chikusa-ku, Nagoya 464-8601 (Japan)

[+] Current address: Department of Chemistry, Faculty of Science Kafr ElSheikh University, 33516 Kafr ElSheikh (Egypt)

[**] This work is supported by the Precursory Research for Embryonic Science and Technology (PRESTO), Japan Science and Technology Agency (JST) (D.J.).

Supporting information for this article is available on the WWW under http://dx.doi.org/10.1002/anie.201209513.

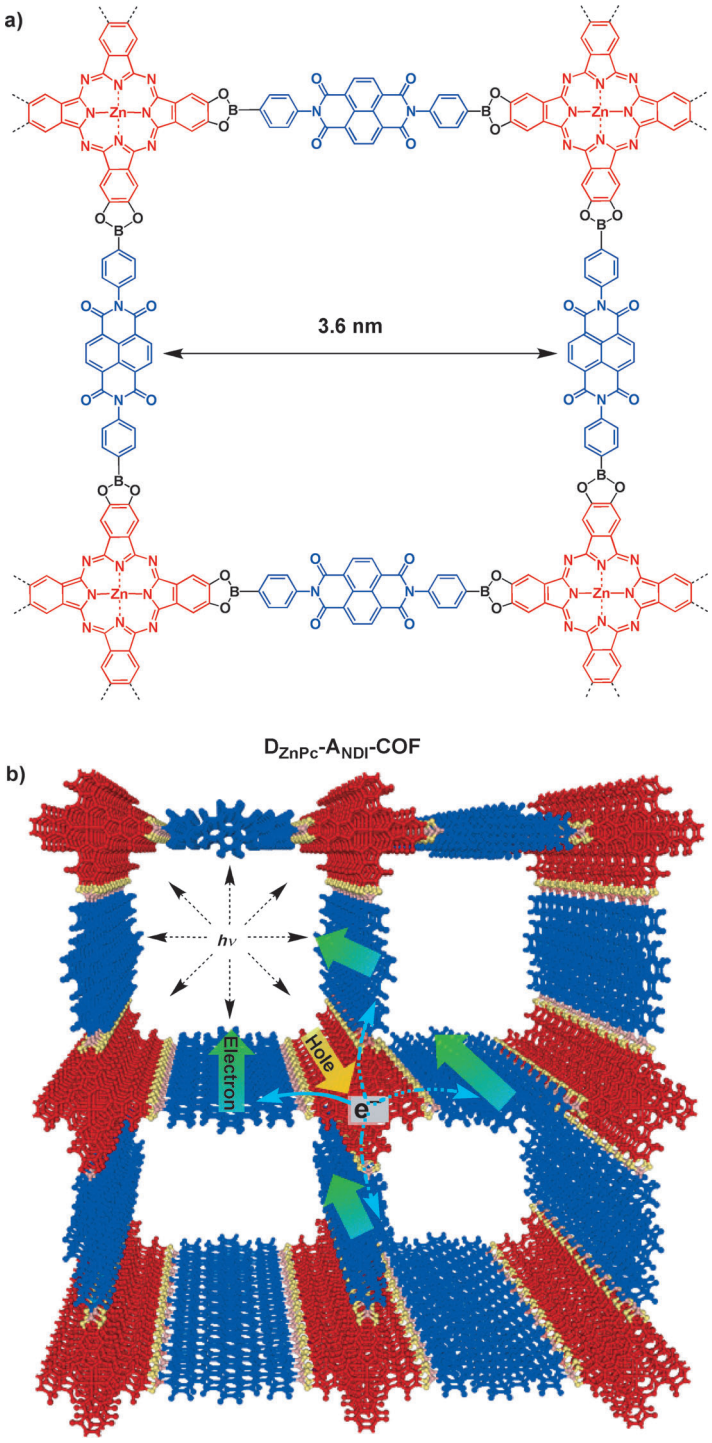

Scheme 1. a) Donor–acceptor COF (D_{ZnPc}-A_{NDI}-COF). Donor and acceptor units are shown in red and blue, respectively. The dotted black lines suggest the extension of periodic structures. b) Illustration of a 2×2 cell of the 0.8 Å slipped AA-stacked COFs and photochemical events.

to 50 nm reveals one type of 3.6 nm-wide mesopores that account for the porosity (Figure 1b).

We resolved the crystalline structure using X-ray diffraction (XRD) measurements in conjunction with structural simulations. The D_{ZnPc}-A_{NDI}-COF exhibited strong XRD peaks at 2.44, 4.96, and 7.54°, which were assigned to the (100), (200), and (300) facets, respectively (Figure 2a, black curve). The peak at 2.44° reveals the periodicity in the XY plane, whereas the peak at 26°, which was assignable to the (001) facet, indicates the periodicity along the *z*-direction with an interlayer spacing of 3.4 Å. The small difference (Figure 2a, blue curve) between the Pawley refinement (Figure 2a, dotted purple curve) and experimental curve supports the above peak assignment. The unit cell parameter of a *P*4 space group is $a = b = 36.1$ Å, $c = 3.4$ Å, and $\alpha = \beta = \gamma = 90°$. The thickness of the COF sample ranged from hundreds of nanometers to 1 μm (see below), which corresponds to thousands of layers stacked in the framework. The simulated XRD pattern based on the 0.8 Å slipped AA-stacking mode reproduced both the experimental XRD peak positions and the peak intensities (Figure 2a, red curve). Scheme 1b shows a 2 × 2 cell of the 0.8 Å slipped AA-stacking mode. In contrast, the staggered AB mode offset by *a*/2 and *b*/2 resulted in an XRD pattern (Figure 2a, green curve) that could not reproduce the curve. The structure of the unit cell shows that the AB-stacking overlaps the pores (Figure 2b,c).

Simulations using the density-functional tight-binding (DFTB) method including the Lennard–Jones (LJ) dispersion revealed that the crystal stacking energy of the 0.8 Å slipped AA-stacking mode is 128.46 kcal mol^{-1} (Table S2). This energy value is slightly greater than that (126.61 kcal mol^{-1}) of the eclipsed AA-stacking and is considerably greater than that (16.02 kcal mol^{-1}) of the staggered AB mode. These energy differences confirmed that the slipped AA-stacking mode is superior to the other modes.

Electron density mapping revealed that the HOMO is centered on the donor unit, whereas the LUMO is localized on the acceptor group (Figure S5a,b). This result indicates that the HOMO and LUMO are suitably paired for electron transfer. Differential-pulse voltammetric measurements of D_{ZnPc}-A_{NDI}-COF dispersed in benzonitrile revealed a one-electron oxidation at 0.42 V, which was attributed to the ZnPc radical cation, and a reduction at −0.52 V, which was assigned to the NDI radical anion (Figure S6). The free-energy change is −0.95 eV, which shows that there is a large exothermic driving force for electron transfer.

Femtosecond transient spectroscopy of a benzonitrile-dispersed D_{ZnPc}-A_{NDI}-COF suspension at 298 K upon laser irradiation at 430 nm yielded an absorption profile with peaks at 540 and 690 nm, which is most likely a mirror image of the steady-state absorption spectrum (Figure S7a). Monitoring at an initial time, for example, 1.4 ps, confirmed the exact mirror image correlation (Figure S7b). Nanosecond transient absorption spectroscopy also exhibited the mirror image traits at early times (e.g., 1.4 μs, Figure S7c). A significant feature of the COF is its negative absorption throughout the time and wavelength ranges of the nanosecond transient spectra (Figure S7d). Mirror-imaged transient spectra have been observed in the photo-induced electron-transfer mechanisms of hybrid systems, including insoluble single-walled carbon

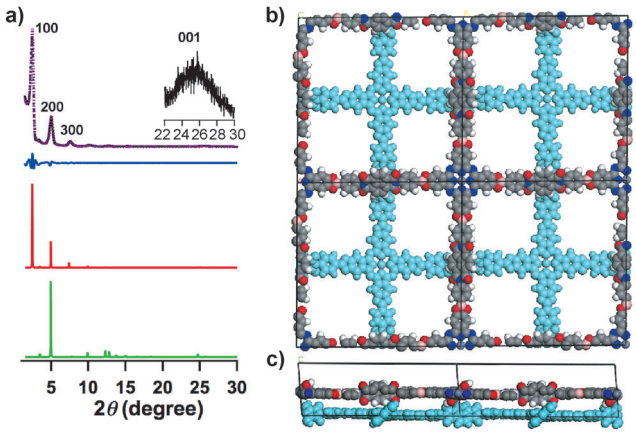

Figure 2. a) XRD patterns of the experimentally observed (black curve), Pawely refined pattern (dotted purple curve), their difference (blue curve), 0.8 Å slipped AA-stacking mode of a *P*1 space group (red curve), and the staggered AB-stacking mode of a *P*1 space group (green curve). The crystal facets are shown with indices on the primary peaks. The slipped AA-stacking mode matches the experimental curve, whereas the staggered AB-stacking mode could not reproduce the experimental profile. b,c) Views of the overlapped unit cell derived from the staggered AB-stacking mode along the b) *z*- and c) *y*-axes.

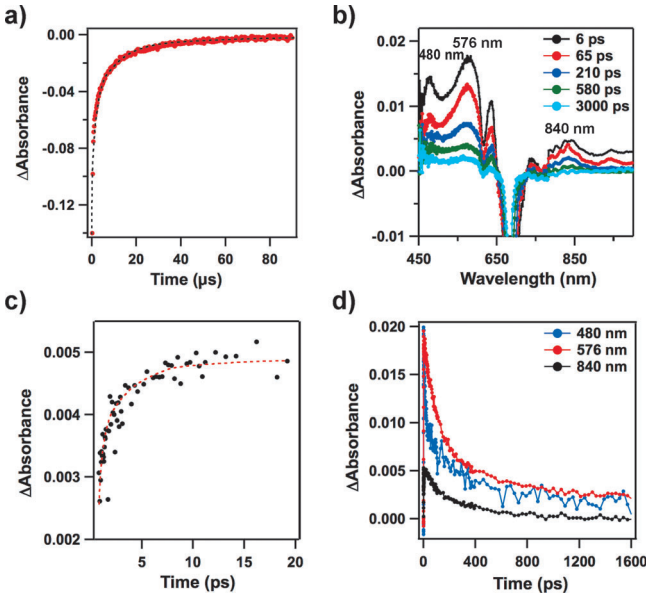

Figure 3. a) The time profile of the nanosecond transient absorption band at 480 nm of a benzonitrile-dispersed COF suspension at 298 K (red dot). The lifetime of the charge-separated state was estimated to be 10 μs using curve fitting (dotted black curve). b) Femtosecond transient absorption spectrum of a COF sample in DMF. The peak at 480 nm are due to the radical anion of the NDI acceptor unit, whereas the peaks at 576 and 840 nm are assignable to the radical cation of the ZnPc donor unit. c) Time profile of the transient band at 840 nm. d) Time profiles of the transient bands at 480, 576, and 840 nm.

nanotubes (SWNTs). The electron delocalization along the long axis of the SWNTs after an electron transfer from tetrathiafulvalenes has been described by the negative imprint of the steady-state absorption spectrum of the SWNT (i.e., the van Hove singularities).[13a] The hole delocalization within the SWNT in an electron-transfer SWNT-coenzyme Q10 system has been identified by the negative transient traits, which show a mirror image of the absorption spectrum of the SWNTs.[13b] Considering these similarities, the transient spectral traits of the COF suggest that a very rapid charge separation occurs within 1.4 ps between the closely positioned donor and acceptor pairs followed by the charge delocalization in the π-columns. The nanosecond transient time profile at 480 nm indicates that the lifetime of the charge-separated state (τ_{CS}) is as long as 10 μs (Figure 3a).[13]

We also performed femto- and nanosecond transient absorption spectroscopic measurements of D_{ZnPc}-A_{NDI}-COF dispersed in a deaerated nonpolar solvent, *o*-dichlorobenzene, at 298 K. The transient absorption spectra exhibited mirror images that were similar to those observed in benzonitrile (Figure S8a,b). The curve fitting of the transient absorption time profiles resulted in a τ_{CS} value of 11 μs (Figure S8c). The long lifetime even in the nonpolar solvent stems from the delocalization of both charges in the bicontinuous columns, which suppress the charge recombination.

Unlike benzonitrile and *o*-dichlorobenzene, *N*,*N*-dimethylformamide (DMF) causes the delamination of the COF layers, which gives rise to an improved solubility and enhanced absorption.[12] Atomic force microscopy measurements confirmed that the delaminated COFs in DMF have a thickness of 3–7 nm, whereas the thickness of the COFs in benzonitrile ranges from several hundred nanometers to 1 μm, which is similar to the thickness of the pristine COF (Figure S9). Transient absorption bands in DMF were observed at 576 and 840 nm, which were assignable to the ZnPc radical cation ($ZnPc^{\bullet+}$), and at 480 nm, which was attributed to the NDI radical anion ($NDI^{\bullet-}$) (Figure 3b and Figure S10). From the time profile of $ZnPc^{\bullet+}$ at 840 nm, the rate of the charge separation process is estimated to be $5.5 \times 10^{11}\ s^{-1}$ (Figure 3c). Therefore, the exciton generation by light absorption is directly coupled with the charge separation through the ultrafast photo-induced electron transfer. Only 1.4 (in benzonitrile) and 1.8 ps (in DMF) are required to complete the electron transfer from the singlet state of ZnPc (^{1}ZnPc*) to NDI and the generation of a charge-separated state with $ZnPc^{\bullet+}$ and $NDI^{\bullet-}$ in the two proximate columns (Scheme 1b). In DMF, the τ_{CS} value was decreased to 217 ps as a result of fewer layers (Figure 3d). In the model electron-transfer compound, π-π-stacked phthalocyanines can extend the lifetime of the charge-separated state because of the charge delocalization in the J-aggregates.[13g] The same ultrafast electron transfer observed for the COFs in different solvents, but with a distinct difference in the lifetime, indicates that the layered structure is crucial for the charge delocalization and the retention of the charge-separated state. In the COFs, the heterojunctions enable an ultrafast charge separation, whereas the bicontinuous π-columns account for the long-distance charge delocalization and long-term charge separation.

To clarify the charge dynamics in the solid-state COFs, we performed time-resolved electron spin resonance spectroscopy (TR-ESR). Before the 700 nm laser flash, the sample was ESR-silent over the entire magnetic field range (Figure 4a,

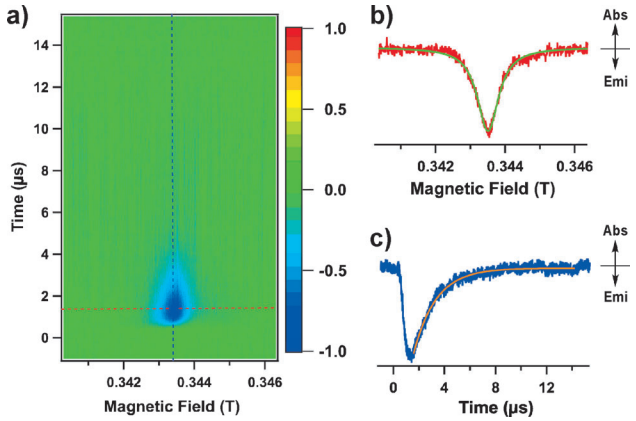

Figure 4. a) Contour plots of the TR-ESR spectrum of the solid-state COF at 280 K. The transverse and longitudinal axes denote the time and magnetic field, respectively. The normal axis is the TR-ESR intensity. The negative and positive signs of the signal intensity indicate the absorption and emission of the microwaves, respectively. b) Time slice of the TR-ESR spectrum at $t = 1.5$ μs. The green line is the line calculated based on the Lorentz function (Abs = absorption and Emi = emission). c) Time profile of the TR-ESR signal at a magnetic field of 0.3435 T. The orange line is the curve calculated based on the exponential function $\Phi = \alpha \exp[-t/\tau_{CS}]$.

$t < 0$ μs). After the laser flash, the TR-ESR signal rapidly increased in intensity as a result of a very rapid charge separation (Figure 4a). The TR-ESR signal exhibited an increase up to $t = 1.5$ μs and then decayed slowly. Therefore, we monitored the TR-ESR spectra at $t = 1.5$ μs as a function of the magnetic field and obtained a time-slice profile, which can be reproduced with a single emission-type Lorentzian with a g value of 2.0059 and a narrow spectral width of 0.75 mT (Figure 4b, green line). The g value of 2.0059 confirms the formation of $ZnPc^{\bullet+}$ and $NDI^{\bullet-}$ species.[14] The narrow spectral width of the COF is consistent with a weak magnetic dipolar interaction between two spins because they are spatially separated and delocalize in the donor and acceptor columns. The TR-ESR measurements at 80 K also confirmed the charge-separated state, as evidenced by a single emission-type Lorentzian profile with the same g value of 2.0059 (Figure S11a,b). Through curve-fitting of the time profiles to an exponential function given by $\Phi = \alpha \exp[-t/\tau_{CS}]$, where α, t, and τ_{CS} are the proportional factor, time, and lifetime, respectively, the τ_{CS} values of the solid-state COFs at 280 and 80 K were determined to be 1.8 and 1500 μs, respectively (Figure 4c, orange line and Figure S11c).

Photo-induced electron transfer and charge separation is a central subject in developing artificial photosynthesis and photoenergy conversion systems. Many efforts have been devoted to highly efficient electron-transfer and charge-separation systems through extensive studies on various model donor–acceptor compounds and on bulk heterojunction systems. The advantage of the donor–acceptor COF configuration over the bulk heterojunction systems is that the COF structure enables the formation of junction between each donor and acceptor unit and the junctions are aligned and periodically ordered throughout the framework. The present study discloses that the donor–acceptor COFs provide a new molecular configuration for electron transfer and charge separation, based on the segregated and bicontinuous donor–acceptor columnar arrays that are controllable through the topological design of the COF skeletons.

In summary, we elucidate the electron transfer and charge dynamics and their structural origin of donor–acceptor COFs through time-resolved spectroscopic studies. In both solvated and solid states, light absorption is directly coupled with exciton generation and charge separation. The heterojunctions in the COFs enable an ultrafast charge separation, whereas the aligned bicontinuous π-columns account for the long-distance charge delocalization and exceptional long-term charge retention. These dynamics provide mechanistic insights into the key photochemical processes involved in optoelectronics and photoenergy conversion systems and suggest that the donor–acceptor COFs are promising high-performance semiconducting materials that may find applications.

Received: November 28, 2012
Published online: January 16, 2013

Keywords: acceptor · charge dynamics · donor · electron transfer · organic frameworks

[1] M. Petty, M. Bryce, D. Bloor in *An introduction to molecular electronics* (Eds.: M. Petty, M. Bryce, D. Bloor), Oxford University Press, New York, **1995**.
[2] J. S. Connolly in *Photochemical conversion and storage of solar energy* (Eds.: J. S. Connolly), Academic Press, New York, **1981**.
[3] P. Heremans, D. Cheyns, B. P. Rand, *Acc. Chem. Res.* **2009**, *42*, 1740–1747.
[4] a) A. P. Côté, A. Benin, N. Ockwig, M. O'Keeffe, A. Matzger, O. M. Yaghi, *Science* **2005**, *310*, 1166–1170; b) A. P. Côté, H. M. El-Kaderi, H. Furukawa, J. R. Hunt, O. M. Yaghi, *J. Am. Chem. Soc.* **2007**, *129*, 12914–12915.
[5] R. W. Tilford, W. R. Gemmill, H. C. zur Loye, J. J. Lavigne, *Chem. Mater.* **2006**, *18*, 5296–5301.
[6] a) X. Feng, X. Ding, D. Jiang, *Chem. Soc. Rev.* **2012**, *41*, 6010–6022; b) A. Nagai, Z. Guo, X. Feng, S. Jin, X. Chen, X. Ding, D. Jiang, *Nat. Commun.* **2011**, *2*, 536; c) S. Wan, J. Guo, J. Kim, H. Ihee, D. Jiang, *Angew. Chem.* **2008**, *120*, 8958–8962; *Angew. Chem. Int. Ed.* **2008**, *47*, 8826–8830; d) S. Wan, J. Guo, J. Kim, H. Ihee, D. Jiang, *Angew. Chem.* **2009**, *121*, 5547–5550; *Angew. Chem. Int. Ed.* **2009**, *48*, 5439–5442; e) X. Ding, J. Guo, X. Feng, Y. Honsho, J. D. Guo, S. Seki, P. Maitarad, A. Saeki, S. Nagase, D. Jiang, *Angew. Chem.* **2011**, *123*, 1325–1329; *Angew. Chem. Int. Ed.* **2011**, *50*, 1289–1293; f) X. Ding, L. Chen, Y. Honsho, X. Feng, O. Saengsawang, J. D. Guo, A. Saeki, S. Seki, S. Irle, S. Nagase, V. Parasuk, D. Jiang, *J. Am. Chem. Soc.* **2011**, *133*, 14510–14513; g) X. Feng, L. Chen, Y. P. Dong, D. Jiang, *Chem. Commun.* **2011**, *47*, 1979–1981; h) X. Feng, L. Liu, Y. Honsho, A. Saeki, S. Seki, S. Irle, Y. P. Dong, A. Nagai, D. Jiang, *Angew. Chem.* **2012**, *124*, 2672–2676; *Angew. Chem. Int. Ed.* **2012**, *51*, 2618–2622; i) X. Feng, L. Chen, Y. Honsho, O. Saengsawang, L. Liu, L. Wang, A. Saeki, S. Irle, S. Seki, Y. P. Dong, D. Jiang, *Adv. Mater.* **2012**, *24*, 3026–3031; j) X. Ding, X. Feng, A. Saeki, S. Seki, A. Nagai, D. Jiang, *Chem. Commun.* **2012**, *48*, 8952–8954; k) X. Feng, Y. P. Dong, D. Jiang, *CrystEngComm* **2013**, *15*, 1508–1511; l) X. Chen, M. Addicoat, S. Irle, A. Nagai, D. Jiang, *J. Am. Chem. Soc.* **2013**, *135*, 546–549.
[7] S. Patwardhan, A. A. Kocherzhenko, F. C. Grozema, L. D. A. Siebbeles, *J. Phys. Chem. C* **2011**, *115*, 11768–11772.

[8] a) E. L. Spitler, W. R. Dichtel, *Nat. Chem.* **2010**, *2*, 672 – 677; b) J. W. Colson, A. R. Woll, A. Mukherjee, M. P. Levendorf, E. L. Spitler, V. B. Shields, M. G. Spencer, J. Park, W. R. Dichtel, *Science* **2011**, *332*, 228 – 231; c) E. L. Spitler, J. W. Colson, F. J. Uribe-Romo, A. R. Woll, M. R. Glovino, A. Saldivar, W. R. Dichtel, *Angew. Chem.* **2012**, *124*, 2677 – 2681; *Angew. Chem. Int. Ed.* **2012**, *51*, 2623 – 2627.

[9] B. Lukose, A. Kuc, T. Heine, *Chem. Eur. J.* **2011**, *17*, 2388 – 2392.

[10] P. Kuhn, M. Antonietti, A. Thomas, *Angew. Chem.* **2008**, *120*, 3499 – 3502; *Angew. Chem. Int. Ed.* **2008**, *47*, 3450 – 3453.

[11] N. L. Campbell, R. Clowes, L. K. Ritchie, A. I. Cooper, *Chem. Mater.* **2009**, *21*, 204 – 206.

[12] I. Berlanga, M. L. Ruiz-González, J. M. González-Calbet, J. L. G. Fierro, R. Mas-Ballesté, F. Zamora, *Small* **2011**, *7*, 1207 – 1211.

[13] a) M. Á. Herranz, C. Ehli, S. Campidelli, M. Gutiérrez, G. L. Hug, K. Ohkubo, S. Fukuzumi, M. Prato, N. Martin, D. M. Guldi, *J. Am. Chem. Soc.* **2008**, *130*, 66 – 73; b) M. Ohtani, S. Fukuzumi, *Chem. Commun.* **2009**, 4997 – 4999; c) A. Sandanayaka, O. Ito, M. Zhang, K. Ajima, S. Iijima, M. Yudasaka, T. Murakami, K. Tsuchida, *Adv. Mater.* **2009**, *21*, 4366 – 4371; d) N. Karousis, J. Ortiz, K. Ohkubo, T. Hasobe, S. Fukuzumi, Á. Sastre-Santos, N. Tagmatarchis, *J. Phys. Chem. C* **2012**, *116*, 20564 – 20573; e) J. E. Bullock, R. Carmieli, S. M. Mickley, J. Vura-Weis, M. R. Wasielewski, *J. Am. Chem. Soc.* **2009**, *131*, 11919 – 11929; f) M. R. Wasielewski, *Acc. Chem. Res.* **2009**, *42*, 1910 – 1921; g) A. Gouloumis, D. González-Rodriguez, P. Vázquez, T. Torres, S. Liu, L. Echegoyen, J. Ramey, G. L. Hug, D. M. Guldi, *J. Am. Chem. Soc.* **2006**, *128*, 12674 – 12684.

[14] T. Nyokong, Z. Gasyma, M. J. Stillman, *Inorg. Chem.* **1987**, *26*, 548 – 553.

